



RESEARCH ARTICLE

Development of a novel hybrid haptic (nHH) device with a remote center of rotation dedicated to laparoscopic surgery

Majdi Meskini^{1,2}, Housseem Saafi^{1,3} , Abdelfattah Mlika¹, Marc Arsicault², Said Zegloul² and Med Amine Laribi² 

¹Mechanical Laboratory of Sousse (LMS), National Engineering School of Sousse, University of Sousse, Sousse, Tunisia, ²Department GMSC—Prime Institute, CNRS—University of Poitiers—ENSMA, Poitiers 86073, France, and ³Preparatory Institute for Engineering Studies of Gafsa, University of Gafsa, Gafsa, Tunisia

Corresponding author: Med Amine Laribi; Email: med.amine.laribi@univ-poitiers.fr

Received: 14 December 2022; **Revised:** 6 May 2023; **Accepted:** 9 June 2023; **First published online:** 25 July 2023

Keywords: haptic devices; laparoscopic surgery; genetic algorithm (GA); optimization problem; simulation; dexterity; serial robots; parallel robots

Abstract

This paper focuses on developing a novel hybrid-haptic (nHH) device with a remote center of rotation with 4 DOFs (degrees of freedom) intended to be used as a haptic device. The new architecture is composed of two chains handling each one a part of the motions. It has the advantages of a parallel robot as high stiffness and accuracy, and the large workspace of the serial robots. The optimal synthesis of the nHH was performed using real-coded genetic algorithms. The optimization criteria and constraints were established and successively formulated and solved using a mono-objective function. A validation and comparison study were performed between the spherical parallel manipulator and the nHH. The obtained results are promising since the nHH is compared to other similar task devices, such as spherical parallel manipulator, and presents a suitable kinematic performance with a task workspace free singularity inside.

1. Introduction

Cooperation between humans and robots plays an important role in many fields. In fact, haptic devices [1, 2] are developed in order to enable its users to interact with software program or a virtual item by giving a force and torque feedback. They are used to increase the application immersion such as gaming [3, 4], training in virtual environment [5–7], and augmented reality [8]. Minimally invasive surgery (MIS) is one of the practical examples where haptic feedback could be very useful [9].

Haptic devices have been widely investigated, and Van den bedem proposed in ref. [10] a spherical serial master haptic device with 4-DoFs. The serial architecture has a simple kinematic. However, it has major drawbacks such as all actuators must be placed on the joint axes which increase the required torques and the weight of the end-effector that the surgeon is asked to support. Several other authors [11] proposed a spherical parallel manipulator (SPM) with a remote center of rotation (CoR) used as a haptic device for MIS (Fig. 1(a)). Contrary to the serial master haptic device, actuators of the SPM are located at the base which reduces the inertia issue of the system. However, this haptic device with parallel architecture suffers from singularities inside his workspace, which causes the loss of DoF and the amplification of errors in the kinematic transformation [12]. In order to cope with the singularity problem inside the workspace of a parallel device, Saafi *et al.* [13] proposed several solutions. Indeed, the behavior of the manipulator is improved by the use of a redundant actuator, the use of an extra sensor, as well as a specific control scheme. As reported by Saafi [14], the use of an extra sensor placed

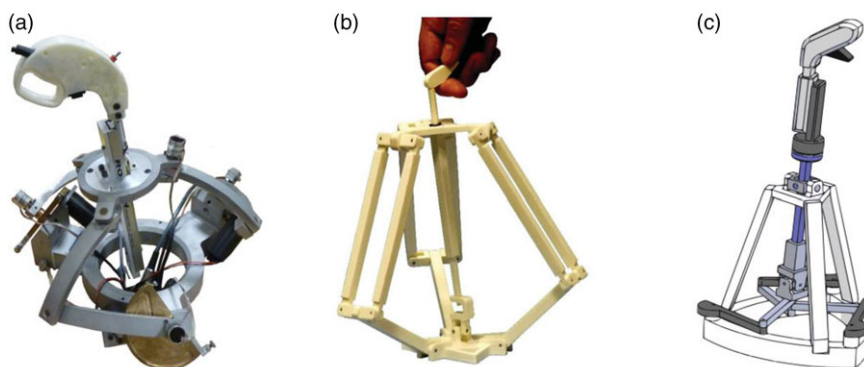


Figure 1. (a): SPM haptic device [23]; (b): haptic device based on Delta robot [17]; (c): hybrid haptic device for laparoscopic surgery [22].

in a passive joint improves the calculation of the forward kinematic model even in singular positions. Another solution is described in refs. [15, 16], which introduce a serial approach for solving the forward kinematic model by placing three sensors on one leg rather than placing them on the actuated joint located at the base. This solution aims to improve the calculation of the forward kinematic model and eliminate the parallel singularity effects in real time application.

Another interesting kinematic of a haptic device was presented by Pérault *et al.* [17]. This architecture is based on Delta robot architecture (Fig. 1(b)). However, the remote CoM of the mechanism is at the bottom of the robot, which increases the gravity compensation and required actuators size.

Hybrid devices as presented in refs. [18–21] started to take their places in a lot of fields. A new hybrid haptic device (Fig. 1(c)) is presented by Saafi *et al.* [22]. This haptic device is the association of a parallel chain and a serial chain. In this latter, the parallel chain is responsible for the tilt motions, and the serial chain handles the self-rotation and the translation. The limitation of this architecture is that the actuator handling the self-rotation should be supported by the serial chain, which increases the weight of the translational part and as consequence the linear actuation torque.

In this paper, a new haptic device with a remote CoR is designed for MIS based on hybrid architecture for laparoscopic surgery. The proposed architecture is based on the association of a parallel part with 3-RRR (R: revolute) parallel planar manipulator, and a serial part connected through universal joint. The self-rotation is supported by the parallel part. The haptic device is optimized in order to guaranty the best kinematic behavior and torque feedback. Simulations are carried out in purpose to validate the manipulator efficiency and handles comparison with other haptic devices.

The paper is organized as follows. In Section 2, the workspace of the desired task will be identified based on the capture of medical expert motions performing MIS. The proposed architecture of the new hybrid haptic (nHH) device is discussed in Section 3. Section 4 is devoted to the dimensional synthesis of the manipulator. In Section 5, a numerical validation and a comparison between the new HH device and the SPM are carried out. Section 6 summarizes this paper.

2. Laparoscopic workspace identification

MIS surgery tools are designed to enter the patient's body through incisions, requiring less time for recovery and less pain for the patient. In order to identify the workspace swept by the instruments during this surgical operation, motion capture system was used to record the gestures of a skilled surgeon [24]. An instance of workspaces deduced from the recorded instruments motions, a clamp and a needle holder, is shown in Fig. 2. Each tool works in a space with a conical geometric form defined by a half-vertex angle α that can go up to 26° .

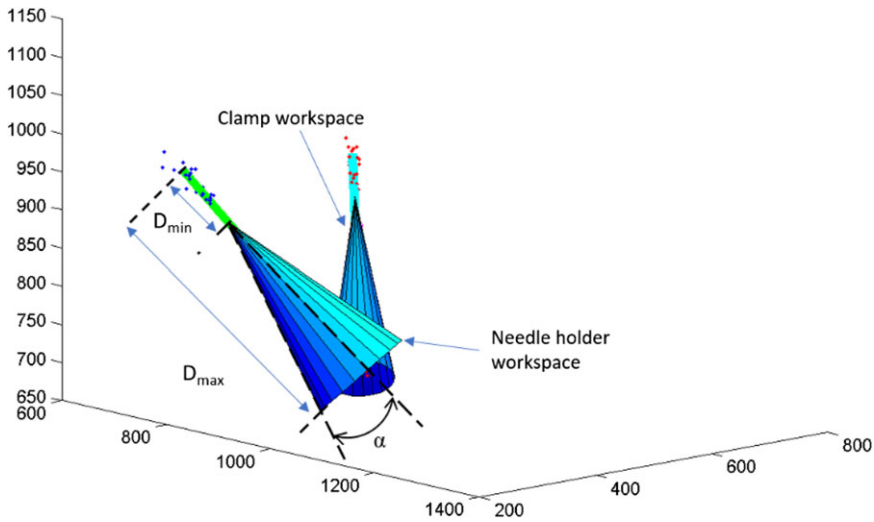


Figure 2. Experimental MIS workspace.

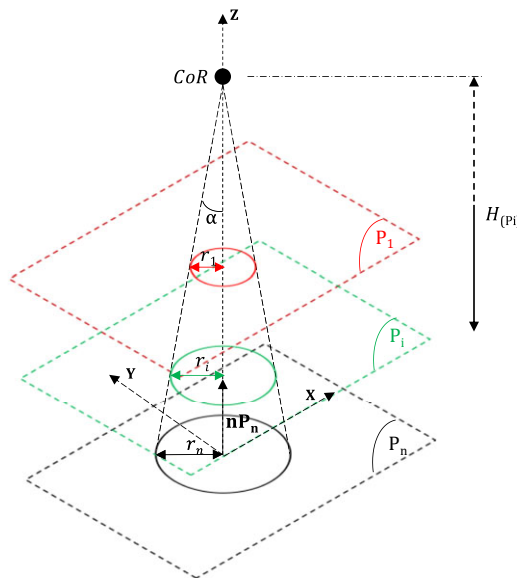


Figure 3. Geometric description of the laparoscopic workspace.

Further, each tool moves along the cone's axis with a translational motion defined by its bounding limits given by the maximal and minimal distances (D_{max} and D_{min}) between the incision point and the tool tip, respectively.

Based on the surgical gestures analysis reported in refs. [25–27], the MIS procedure requires four degrees of freedom, namely three rotations and one translation. One can conclude that the tool workspace is described by a cone with a maximum vertex angle of 26° and a translation of 112 mm along the tool axis direction, respectively.

The geometric construction of the tool workspace given in Fig. 3 shows the location of the CoR, at the top of the cone, and the intersections with a set of parallel planes P_i ($i \in \{1, 2, \dots, n\}$) defined by their common normal vector $\mathbf{n}P_n$. Each plane P_i is located at the distance H_{P_i} , between the plane P_i which

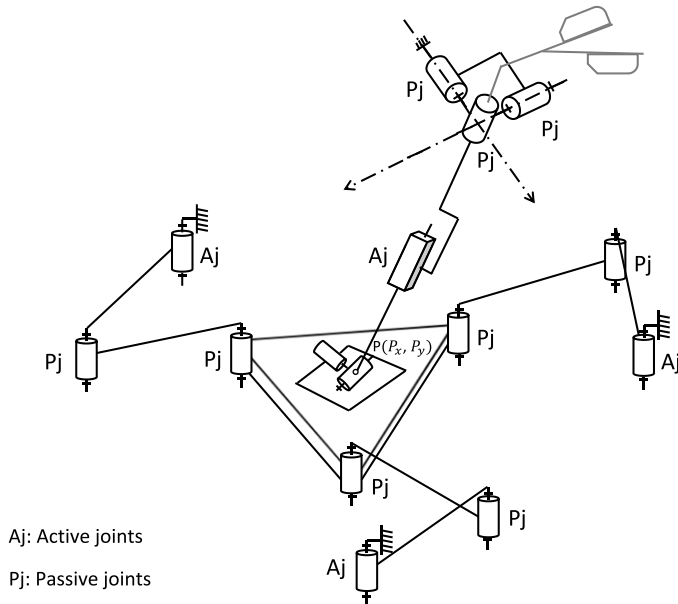


Figure 4. nHH device kinematics.

design the plane of the parallel chain and the CoR. The intersections are described by a set of circles with radius r_i and given by Eq. (1):

$$r_i = H_{(P_i)} \cdot \tan \alpha \tag{1}$$

The next section will introduce the kinematic of the new haptic device for the MIS, called hybrid haptic device.

3. nHH-device

The new proposed architecture, the novel hybrid haptic (nHH) device offers four possible motions as presented in Fig. 4. One can note three rotations around a defined CoR and one translation. This architecture is composed of a serial and a parallel kinematic chain. Each of these chains operates a part of the device. The parallel chain is composed of a 3-RRR planar manipulator with 3 DoFs, which allows to handle the two tilt motions and the self-rotation. The serial chain is composed of a prismatic and spherical joint, allowing to manipulate the translation around a fixed CoR. The two chains of this device are connected through a universal joint. This association allows to overcome with the drawbacks of the serial architectures where the actuators are placed on the joint axes and increase the moving masses which alters dynamic behavior.

In the section below, the two kinematic chains of the presented architecture will be discussed in detail. The CAD model of the nHH device and its developed prototype are presented in Fig. 5(a) and (b), respectively.

3.1. Serial chain (SC)

A universal joint serving as a CoR, a revolute joint for self-rotation, and a prismatic joint to control the linear displacement defined by T make up the serial chain of the proposed nHH device. As shown in Fig. 6(a), the orientations of the serial chain are specified using cardon angles with three different rotations in three-dimensional space. The bond graph of the serial chain is presented in Fig. 6(b).

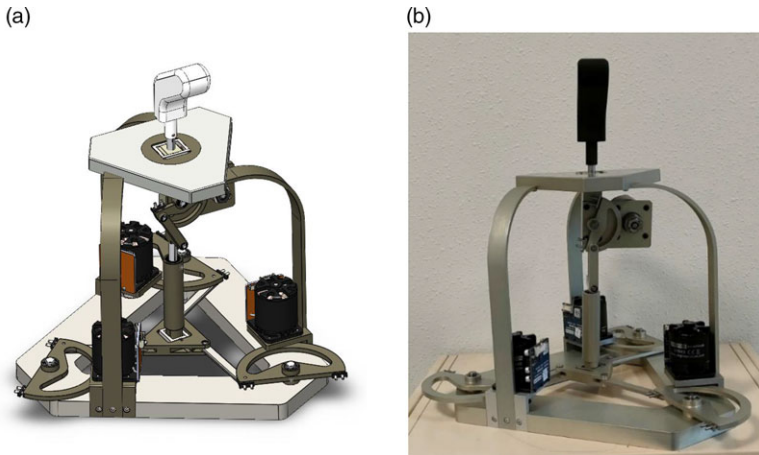


Figure 5. (a): CAD model of the nHH device. (b): nHH device prototype.

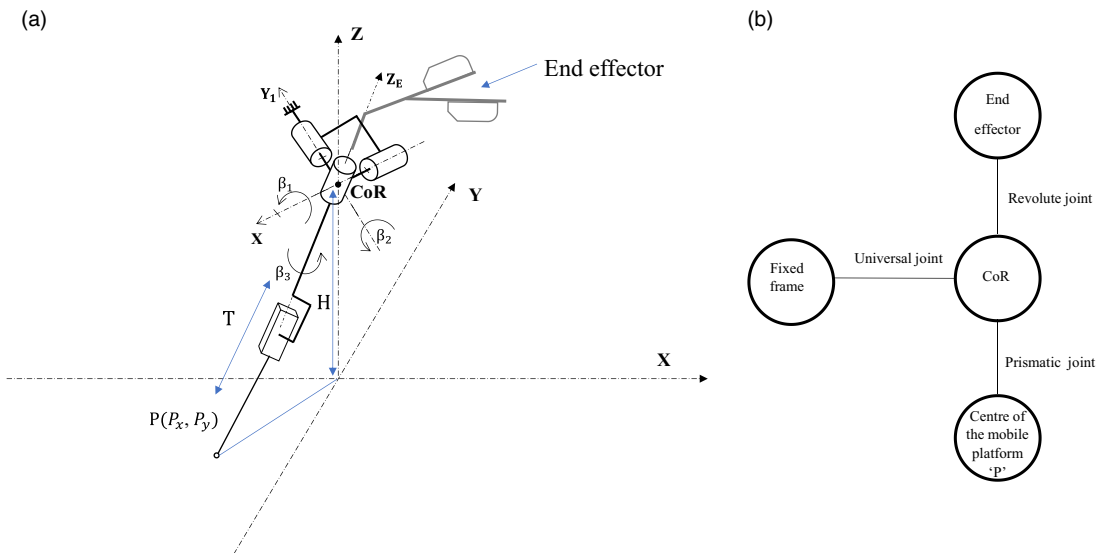


Figure 6. (a): Serial chain architecture of the nHH device; (b): serial chain bond graph.

The end effector velocity can be expressed using the universal joints $(\beta_1, \beta_2, \beta_3)$ presented in Fig. 6 by Eq. (2):

$$\omega_{EF} = \dot{\beta}_1 \mathbf{X} + \dot{\beta}_2 \mathbf{Y}_1 + \dot{\beta}_3 \mathbf{Z}_E \tag{2}$$

$$\begin{pmatrix} \omega_x \\ \omega_y \\ \omega_z \end{pmatrix} = \mathbf{J} \mathbf{s} \begin{pmatrix} \dot{\beta}_1 \\ \dot{\beta}_2 \\ \dot{\beta}_3 \end{pmatrix} \tag{3}$$

The orientation of end effector in workspace can be also described by the Euler angles (ψ, θ, ϕ) with ZXZ convention. In this case the angular velocity of the end effector can be expressed as follows:

$$\omega_{EF} = \dot{\psi} \mathbf{Z} + \dot{\theta} \mathbf{X}_1 + \dot{\varphi} \mathbf{Z}_E \tag{4}$$

$$\begin{pmatrix} \omega_x \\ \omega_y \\ \omega_z \end{pmatrix} = \begin{bmatrix} 0 & \cos \psi & \sin \theta \sin \psi \\ 0 & \sin \psi & -\sin \theta \cos \psi \\ 1 & 0 & \cos \theta \end{bmatrix} \begin{pmatrix} \dot{\psi} \\ \dot{\theta} \\ \dot{\varphi} \end{pmatrix} \tag{5}$$

Or from Eq. (3) and Eq. (5) we can obtain:

$$\begin{bmatrix} 0 & \cos \theta & -\cos \theta \sin \psi \\ 0 & \sin \theta & \sin \theta \\ 1 & 0 & \cos \theta \end{bmatrix} \begin{pmatrix} \dot{\psi} \\ \dot{\theta} \\ \dot{\varphi} \end{pmatrix} = \mathbf{J} \mathbf{s} \begin{pmatrix} \dot{\beta}_1 \\ \dot{\beta}_2 \\ \dot{\beta}_3 \end{pmatrix} \tag{6}$$

$$\begin{pmatrix} \dot{\psi} \\ \dot{\theta} \\ \dot{\varphi} \end{pmatrix} = \begin{bmatrix} 0 & \cos \theta & -\cos \theta \sin \psi \\ 0 & \sin \theta & \sin \theta \\ 1 & 0 & \cos \theta \end{bmatrix}^{-1} \mathbf{J} \mathbf{s} \begin{pmatrix} \dot{\beta}_1 \\ \dot{\beta}_2 \\ \dot{\beta}_3 \end{pmatrix} \tag{7}$$

where

$$\mathbf{J} \mathbf{s} = [\mathbf{X} \ \mathbf{Y}_1 \ \mathbf{Z}_E] . \tag{8}$$

with,

$$\begin{cases} \mathbf{Y}_1 = R_x(\beta_1) \ \mathbf{Y} \\ \mathbf{Z}_E = R_z(\psi) R_x(\theta) R_z(\varphi) \ \mathbf{Z} \end{cases} \tag{9}$$

Using the identification between the Euler matrix and the cardan matrix, β_1 can be expressed using Euler angles by Eq. (11):

$$\beta_1 = \tan^{-1}(\cos \psi \tan \theta) \tag{11}$$

Using this result, the $\mathbf{J} \mathbf{s}$ matrix is expressed by

$$\mathbf{J} \mathbf{s} = \begin{bmatrix} 1 & 0 & \sin(\psi) \sin(\theta) \\ 0 & \cos(\tan^{-1}(\cos \psi \tan \theta)) & -\cos \psi \sin(\theta) \\ 0 & \sin(\tan^{-1}(\cos \psi \tan \theta)) & \cos(\theta) \end{bmatrix} \tag{12}$$

The matrix $\mathbf{J} \mathbf{s}$ of the serial chain is used in the evaluation of the kinematic performance of the serial chain. This evaluation is based on the dexterity criterion, detailed in Section 3.2.2. The dexterity noted μ_s is equal to the inverse of the conditioning number of the matrix $\mathbf{J} \mathbf{s}$ (Eq. 13).

$$\mu_s = \frac{1}{K(\mathbf{J} \mathbf{s})} \tag{13}$$

The dexterity distribution in the plane (ψ, θ) of the serial chain is presented in Fig. 7. One can conclude suitable kinematic performances of the serial chain since the dexterity is higher than 0.5 over the whole workspace.

3.2. Parallel chain (PC)

3.2.1. Kinematic model

The parallel chain of the nHH device is defined by a 3-RRR parallel planar manipulator. This latter is composed of three identical kinematic chains connecting a mobile platform to a fixed base. Each chain is consisting of an actuated revolute joint attached to the ground followed by two revolute joints to be connected to the platform, as shown in Fig. 8.

The center of the joint connecting the two links of the i th chain will be referred to as B_i . The length of the links of the i th chain will be noted L_1 (for link $A_i B_i$) and L_2 (for link $B_i C_i$). The active and passive revolute joints are denoted by θ_i and β_i , respectively, with $i = 1, 2, 3$.

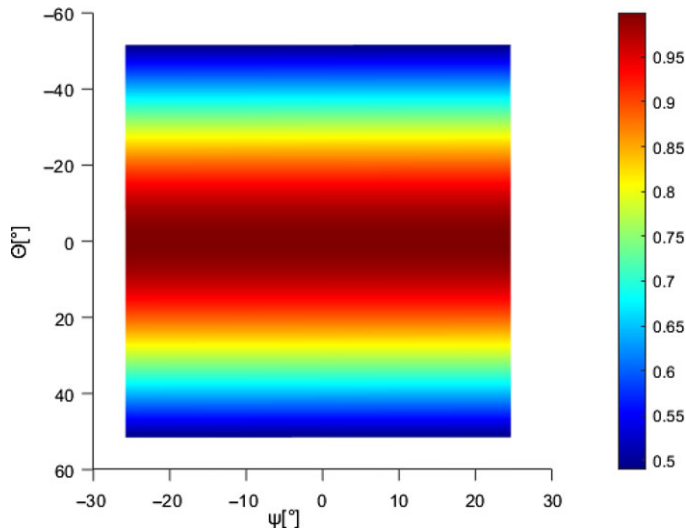


Figure 7. Dexterity distribution of the serial chain in the (ψ, θ) plane.

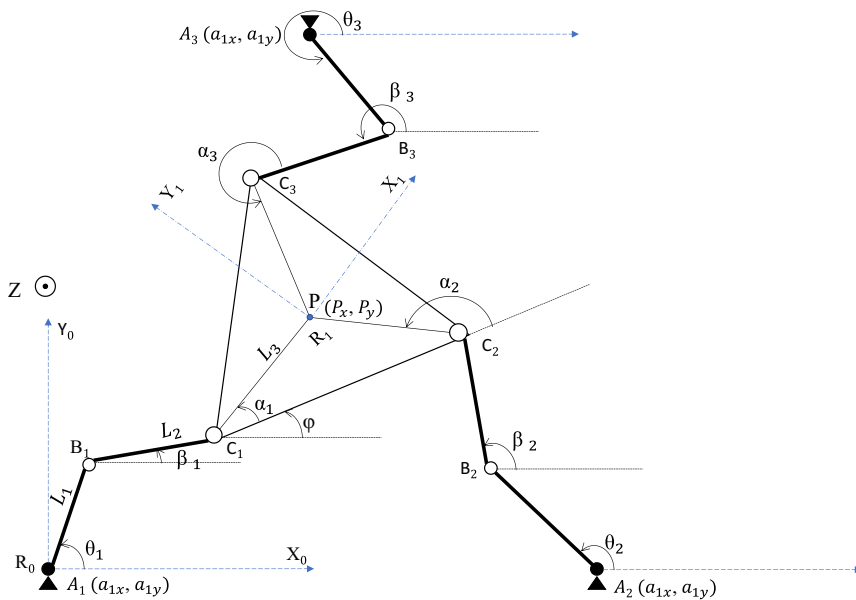


Figure 8. Geometric parameters of the parallel chain (3-RRR) of the nHH device.

The position of the moving platform is defined by the coordinates of point $P(P_x, P_y)$ in the fixed reference frame R_0 and its orientation is given by the angle φ between one axis of the fixed reference frame and the corresponding frame R_1 of the moving frame, as show on Fig. 8.

The inverse geometric model, to obtain the active joints from the position and the orientation of the moving platform, can be expressed as follows [28]:

$$\theta_i = 2 \tan^{-1} \frac{-\bar{N}_i \pm \sqrt{\bar{M}_i^2 + \bar{N}_i^2 - \bar{L}_i^2}}{\bar{L}_i - \bar{M}_i} \tag{14}$$

where

$$\bar{M}_i = 2a_{ix}L_1 + 2L_1L_3 \cos(\varphi + \alpha_i) - 2P_xL_1 \quad (15)$$

$$\bar{N}_i = 2a_{iy}L_1 + 2L_1L_3 \sin(\varphi + \alpha_i) - 2P_yL_1 \quad (16)$$

$$\begin{aligned} \bar{L}_i = & a_{ix}^2 + a_{iy}^2 + P_x^2 + P_y^2 + L_1^2 + L_3^2 + 2a_{ix}L_3 \cos(\varphi + \alpha_i) - 2a_{ix}P_x - 2P_xL_3 \cos(\varphi + \alpha_i) \\ & + 2a_{iy}L_3 \sin(\varphi + \alpha_i) - 2a_{iy}P_y - 2P_yL_3 \sin(\varphi + \alpha_i) - L_2^2. \end{aligned} \quad (17)$$

The kinematic model of the 3-RRR parallel planar manipulator can be computed by the derivation of the forward kinematic model presented by the following equations [28]:

$$\mathbf{OP} = \mathbf{OA} + \mathbf{AB} + \mathbf{BC} + \mathbf{CP} \quad (18)$$

$$P_x = a_{ix} + L_1 \cos \theta_i + L_2 \cos \beta_i + L_3 \cos(\varphi + \alpha_i) \quad (19)$$

$$P_y = a_{iy} + L_1 \sin \theta_i + L_2 \sin \beta_i + L_3 \sin(\varphi + \alpha_i) \quad (20)$$

To finally obtain an equation expressed as follows:

$$\mathbf{J}_\theta \dot{\theta} = \mathbf{J}_x \dot{X}$$

where \mathbf{J}_x and \mathbf{J}_θ are the parallel part and the serial part of the Jacobian matrix presented by Eqs. (21) and (22), respectively.

$$\mathbf{J}_x = \begin{bmatrix} Jx_1 & Jy_1 & Jz_1 \\ Jx_2 & Jy_2 & Jz_2 \\ Jx_3 & Jy_3 & Jz_3 \end{bmatrix}; \quad (21)$$

$$\mathbf{J}_\theta = \begin{bmatrix} J\theta_1 & 0 & 0 \\ 0 & J\theta_2 & 0 \\ 0 & 0 & J\theta_3 \end{bmatrix}; \quad (22)$$

where

$$Jx_i = 2P_x - 2a_{ix} - 2L_3 \cos(\varphi + \alpha_i) - 2L_1 \cos(\theta_i) \quad (23)$$

$$Jy_i = 2P_y - 2a_{iy} - 2L_3 \sin(\varphi + \alpha_i) - 2L_1 \sin(\theta_i) \quad (24)$$

$$\begin{aligned} Jz_i = & 2L_3a_{iy} \cos(\varphi + \alpha_i) - 2L_3a_{ix} \sin(\varphi + \alpha_i) - 2L_3P_y \cos(\varphi + \alpha_i) \\ & + 2L_3P_x \sin(\varphi + \alpha_i) - 2L_1L_3 \sin(\varphi + \alpha_i) \cos(\theta_i) - 2L_1L_3 \sin(\varphi + \alpha_i) \sin(\theta_i) \end{aligned} \quad (25)$$

$$\begin{aligned} J\theta_i = & 2L_1P_x \sin(\theta_i) + 2L_1a_{iy} \cos(\theta_i) - 2L_1a_{ix} \sin(\theta_i) - 2L_1P_y \cos(\theta_i) \\ & + 2L_1L_3 \sin(\varphi + \alpha_i) \cos(\theta_i) - 2L_1L_3 \cos(\varphi + \alpha_i) \sin(\theta_i) \end{aligned} \quad (26)$$

The Jacobian matrix satisfies Eq. (27):

$$\mathbf{J}_p = \mathbf{J}_\theta^{-1} \mathbf{J}_x \quad (27)$$

3.2.2. Dexterity

In order to evaluate the kinematic performance of the parallel chain of the nHH device, the dexterity will be examined. This criterion allows to measure how far the moving platform is far from singularity inside

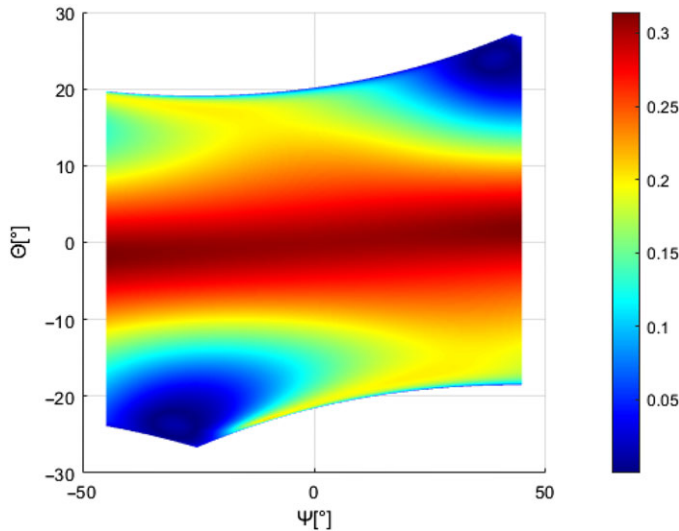


Figure 9. Dexterity distribution of Parallel chain in the plane (ψ, θ) with self-rotation $\phi = -20^\circ$.

the workspace and one of the most considered criteria in literature [29]. The dexterity is computed using the inverse of the condition number described by Eq. (28).

$$\mu_p = \frac{1}{K(\mathbf{J}_p)} \tag{28}$$

where, $K(\mathbf{J}_p) = \|\mathbf{J}_p\| \cdot \|\mathbf{J}_p^{-1}\|$

In order to evaluate the global dexterity inside a desired workspace, the global conditioning index will be considered and defined as follows [30]:

$$\mu_p^G = \frac{\sum_{i=1}^N \mu_{pi}}{N} \tag{29}$$

N : discretization parameter of the desired workspace.

In order to identify the coupling between the serial and the parallel chain of the nHH device, the relations between the cartesian coordinates of the center of the moving platform of the parallel chain and the orientation of the serial chain are determined. As shown on Fig. 6, these relations are defined by Eqs. (30) and (31):

$$\begin{cases} P_x = -H \tan \theta \cos \psi & (30) \\ P_y = -H \tan \theta \sin \psi & (31) \end{cases}$$

For each orientation ψ and θ leading to a position of the moving platform, the active angles $(\theta_1, \theta_2, \theta_3)$ can be computed using the inverse kinematic model presented in Section 3.2. As consequence, the dexterity distribution of the parallel chain can be obtained by a simple mapping in the (ψ, θ) plane and given in the Figs. 9, 10 and 11 for different values of the self-rotation.

4. Dimensional synthesis of the nHH device

The aim of this section is to identify the best design parameters of the nHH device leading to the best trajectory tracking accuracy. This latter can be characterized by the kinematic performance of the nHH device. The value of this performance depends on the positioning error, between the articulate coordinates and the operational ones, due to the kinematic transformations.

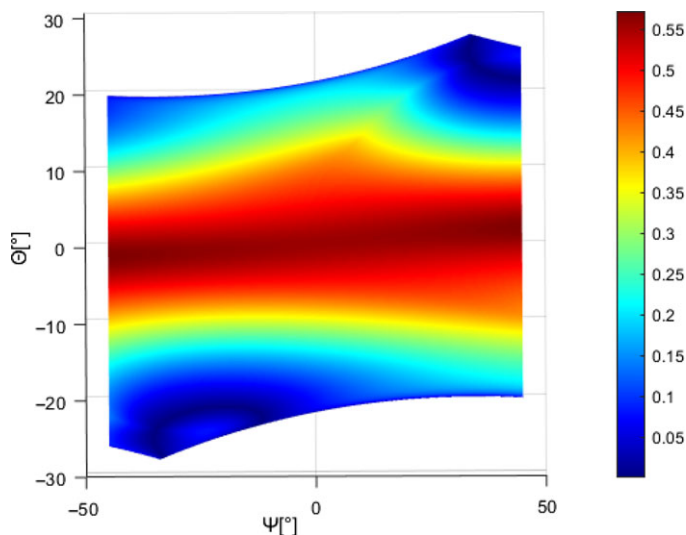


Figure 10. Dexterity distribution of parallel chain in the plane (ψ, θ) with self-rotation $\phi = 0^\circ$.

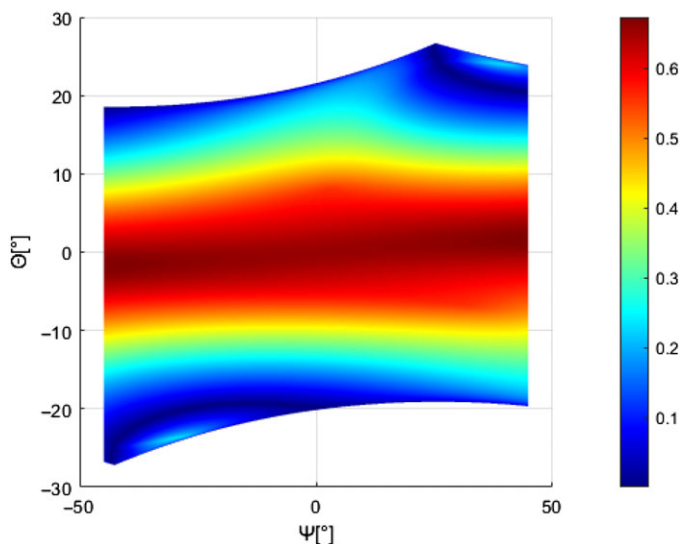


Figure 11. Dexterity distribution of parallel chain in the plane (ψ, θ) with self-rotation $\phi = 20^\circ$.

The optimization process, based on the dimensional synthesis, allows identifying the nHH device that is more suitable for the criteria selected by the user and in our case the kinematic performance. In the literature, several methods and indices can be found [29, 31, 32] To compute the kinematic performance of a structure, we chose the global dexterity defined by Gosselin [29] as it characterizes the isotropy of the robot velocity.

4.1. Problem formulation

This section focuses on the development and the results of the multidimensional, nonlinear optimization problem of selecting the geometric design variables for the nHH device having a specified workspace

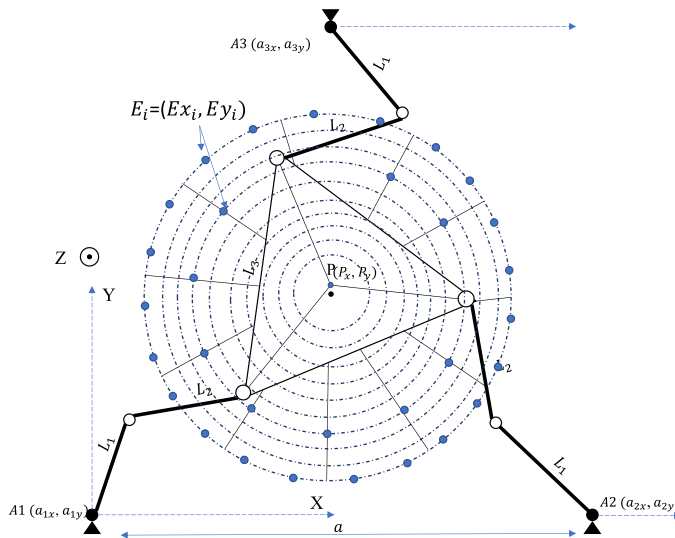


Figure 12. Intersection between the cone and the parallel chain plane.

as well as the best dexterity distribution. The aimed application is the minimally invasive surgery due to the experimental recorded path used in the comparison study in Section 5 but can be enlarged to others.

Figure 12 presents the intersection between the cone and the plane crossing the parallel chain. This intersection is bounded by a circle C and discretized in n point E_i .

The proposed approach is based on the minimization of the objective function $M(\mathbf{L})$, which reflects the overall performance of the manipulator by associating two separate indexes for the parallel chain and the serial chain with giving more weight to the parallel part, since the serial chain has a good performance even at the edges of the workspace. Indeed, the performance of the whole device is related to each chain and the performance of the device can reach a good level only when the performance of both parts is good. By this association, we manage to have a performance indicator of the whole manipulator. This approach is based on using a genetic algorithm (GA) method [33–35]. The optimization problem is stated as follows:

$$\text{Minimise } M(\mathbf{L}) = \sigma \cdot \bar{\mu}_P(\mathbf{L}) + (1 - \sigma) \cdot \bar{\mu}_S(\mathbf{L}) \tag{32}$$

Subject to,

$$W_E = \sum_{j=1}^3 \sum_{i=1}^n P_j(E_i) \leq 0 \tag{33}$$

With

$$P_j(E_i) = (E_{xi} - a_{ix})^2 + (E_{yi} - a_{iy})^2 - (L_1 + L_2 + L_3 - \delta)^2 \tag{34}$$

$$u_k \in [u_{k \min}; u_{k \max}]$$

$$u_{k=\{1,5\}} = \{L_1 \ L_2 \ L_3 \ aH\}; \mathbf{V} = [L_1 \ L_2 \ L_3 \ aH]^T$$

where

$\bar{\mu}_P(\mathbf{L}) = \frac{1}{N} \sum_{i=1}^N \mu_i(\mathbf{L})$: global dexterity of the parallel manipulator.

$\bar{\mu}_S(\mathbf{L}) = \frac{1}{N} \sum_{i=1}^N \mu_i(\mathbf{L})$: global dexterity of the serial chain.

σ : weighting coefficient ($0 < \sigma < 1$). $\sigma = 0.7$.

$P_j(E_i)$: constraint of the existence of the workspace.

$M(\mathbf{L})$: Objective functions defining the criteria, the kinematic performance, to optimize.

Table I. Bounding intervals of the parallel chain design parameters.

	L_1	L_2	L_3	a	H
UB [mm]	10	10	20	100	100
LB [mm]	100	100	70	300	250

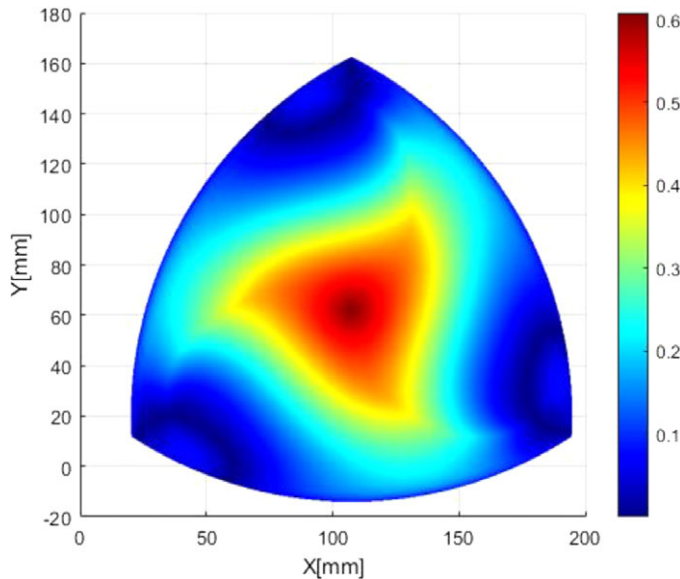


Figure 13. Dexterity distribution of the PC at $\varphi = 0^\circ$.

\mathbf{V} : Design vector of the parallel chain with the length L_i ; $i \in \{1,2,3\}$, the distance a representing the dimension of the base and the distance H between the PC plane and the CoR.

δ : the safety margin for singularity avoidance.

4.2. Genetic algorithm method, optimization and results

GAs are heuristic search algorithms based on the mechanism of natural selection and natural genetics initially proposed by Holland [36]. They have been used in a variety of engineering fields such as in machine design. A real-coded GA [37] is used here to solve the optimization problem.

In the present application, each individual is a design vector, $\mathbf{L} = [L_1 L_2 L_3 a H]^T$. It corresponds to the nHH manipulator, and its characteristics are design parameters. A population of 50 individuals is manipulated through 300 generations.

The algorithm is allowed to select the optimal values of the design parameters in the bounding intervals given in Table I.

The optimal design vector \mathbf{L}_{op} obtained using the GA is presented by the following:

$$\mathbf{L}_{op} = [80 \ 80 \ 70 \ 215 \ 125]^T$$

The figure below represents the dexterity distribution of the parallel chain within its workspace in the plane (X, Y) with a self-rotation of the moving platform equal to 0° .

The optimization of the serial chain is obtained by optimizing the distance H between plan of the parallel chain and the CoR. In fact, as mentioned in the Section 2, the projection of the cone in the parallel chain plane yields to a circular border defined by E_i (Fig. 13) with the radius linked to the distance H . The coordinates of the points E_i are given by Eq. (35).

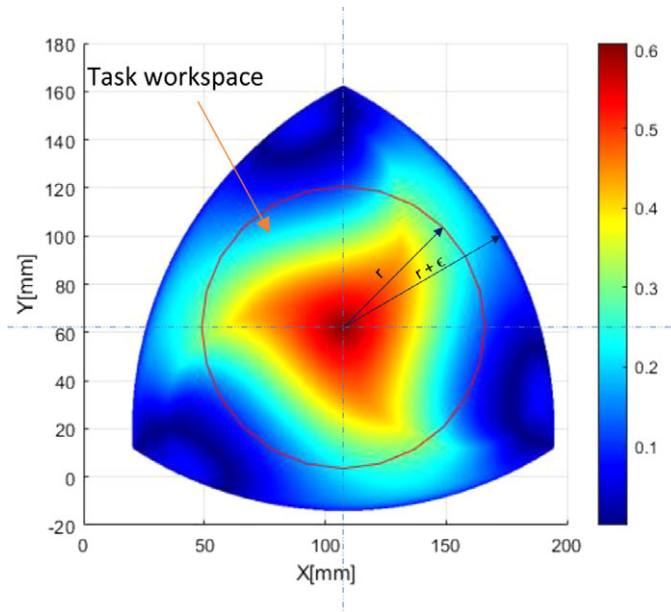


Figure 14. Task workspace in the PC plane.

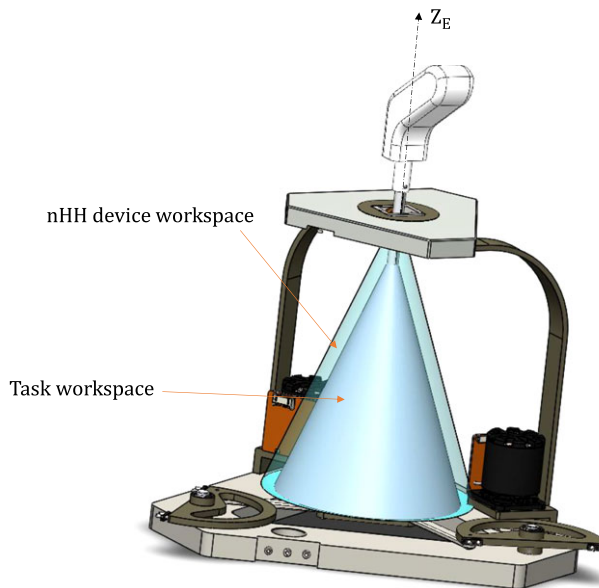


Figure 15. 3D representation of the task workspace and the nHH workspace.

$$E_i = \begin{cases} E_{xi} = r \cdot \cos \rho \\ E_{yi} = r \cdot \sin \rho \end{cases} \quad \text{for } \rho = \left[0, : \frac{\pi}{12} : 2\pi \right] \quad (35)$$

With

$$r = 61 \text{ mm}$$

Figures 14 and 15 give a visual representation of the task workspace in the PC plane and 3D representation of the workspace with nHH device, respectively.

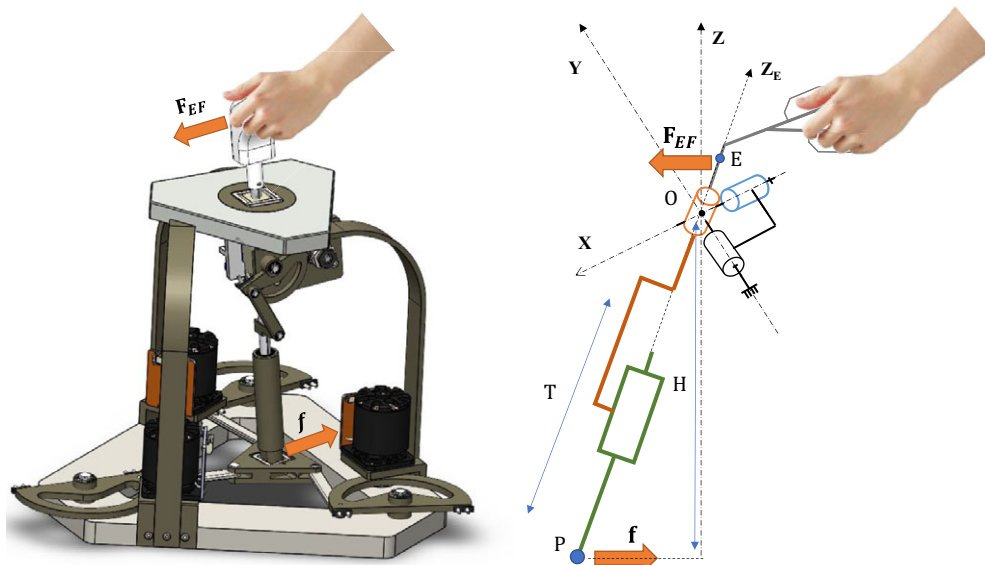


Figure 16. Applied efforts on the nHH device.

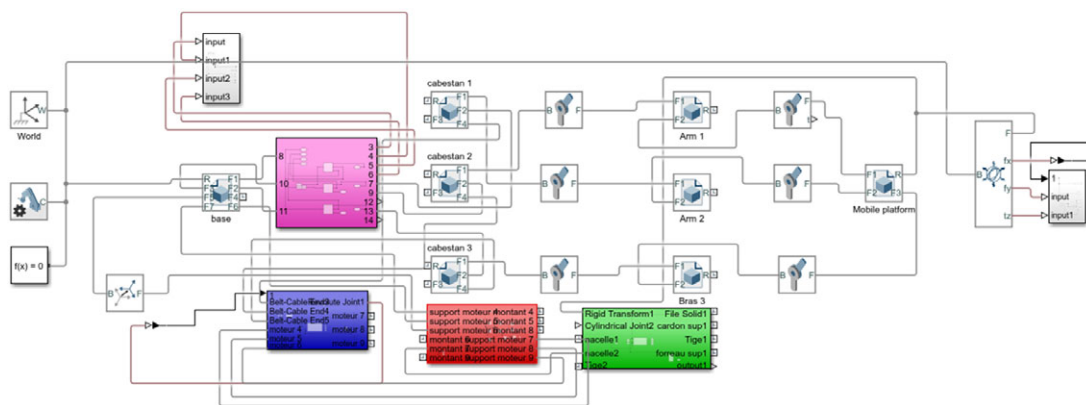


Figure 17. Validation model: Simscape model of the nHH device.

5. Numerical validation of haptic feedback and comparison

The nHH device represents the master station of a master–slave platform. This device is used to control the slave robot and ensure the force feedback in case of the slave robot interaction with its external environment. The nHH device is designed using a mechanical solution based on a capstan associated with a simplex DC motor. A set of four capstans and four simplex DC motors can be observed on the prototype. The capstan for the revolute joint is with a ratio of 4.1 and the one for the translation is with a ratio of 3.4. Regarding the actuation, the DC motors present a nominal torque of 0.8 [Nm]. The first numerical validation is presented in this section and in future works, the experimental study will be developed and validated. So, in order to validate the kinematic performance of the optimal solution, in this section the model of the nHH device is developed using a SimMechanics model based on rigid-body dynamics according to the scenario presented in Figs. 16 and 17. For different configuration $N(N_x, N_y)$ of the nHH as presented in Fig. 18, we determine the feedback force on the end-effector by applying the

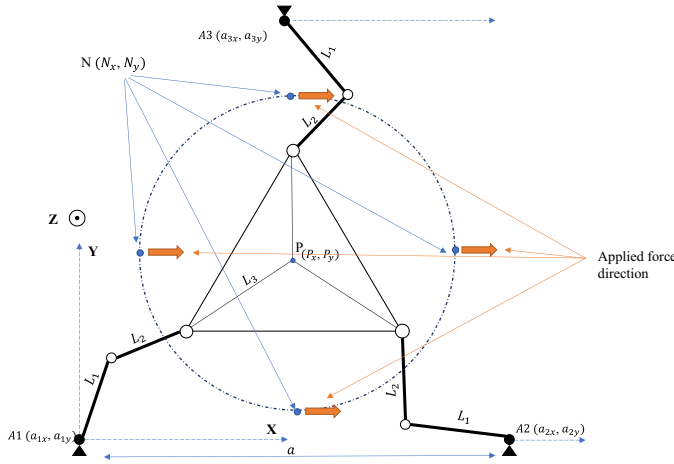


Figure 18. Configurations of nHH.

torques on the actuated joints. In addition, a comparison study is performed to prove the efficiency of the proposed architecture of nHH device.

The nHH device is assumed to be a rigid body; therefore, deformations are not considered in this study. A function that calculates the actuated joint torques is constructed. The inputs to this function are the references forces \mathbf{F}_{EF} and \mathbf{f} , which are the force vector applied on the end effector of the mobile parallel platform as presented in Fig. 16, respectively.

The analytic method to compute the actuated joint torques of the parallel chain for a given reference force \mathbf{f} is defined by the following relation:

$$\boldsymbol{\tau} = \mathbf{J}_p^T \cdot \mathbf{f} \tag{36}$$

with

\mathbf{f} : force applied on the parallel mobile platform, $\mathbf{f} = [f_x \ f_y \ m_z]^T$.

\mathbf{J}_p^T : Transpose of the Jacobian matrix of the parallel manipulator.

$\boldsymbol{\tau}$: Actuated joints torque, $\boldsymbol{\tau} = [\tau_1 \ \tau_2 \ \tau_3]^T$.

The input are the actuated joints torques calculated using the equation above. The output is the applied force on the end effector.

The relation between the two efforts is denoted by Eq. (37). The joint torque is inserted into the SimMechanics model to compute the force \mathbf{F}_{EF} , for different configurations.

$$\mathbf{OE} \wedge \mathbf{F}_{EF} = \mathbf{OP} \wedge \mathbf{f} \tag{37}$$

with

$$\mathbf{F}_{EF} = \begin{pmatrix} F_x \\ F_y \\ M_z \end{pmatrix}, \mathbf{f} = \begin{pmatrix} f_x \\ f_y \\ m_z \end{pmatrix}, \mathbf{OE} = \begin{pmatrix} x_E \\ y_E \\ z_E \end{pmatrix}, \mathbf{OP} = \begin{pmatrix} x_p \\ y_p \\ z_p \end{pmatrix};$$

For $M_z = m_z = 0$, the relation between the applied effort on the end effector and the mobile platform is given by the equations below:

$$\begin{cases} F_x = \frac{z_p}{z_E} \cdot f_x \\ F_y = \frac{z_p}{z_E} \cdot f_y \end{cases} \tag{38}$$

$$\begin{cases} F_x = \frac{z_p}{z_E} \cdot f_x \\ F_y = \frac{z_p}{z_E} \cdot f_y \end{cases} \tag{39}$$

Table II resume the applied torques, analytic force value, and the simulation force value on the end effector for the four different configurations $N(N_x, N_y)$ at the edges of the workspace as presented in

Table II. Force values depending on nHH configuration.

	N_x [M]	N_y [M]	Analytic force value [N]	Simulation force value [N]
Position 1	0.121	0.030	1	0.98
Position 2	0.121	0.083	1	1.0065
Position 3	0.140	0.075	1	1.021
Position 4	0.095	0.075	1	0.94

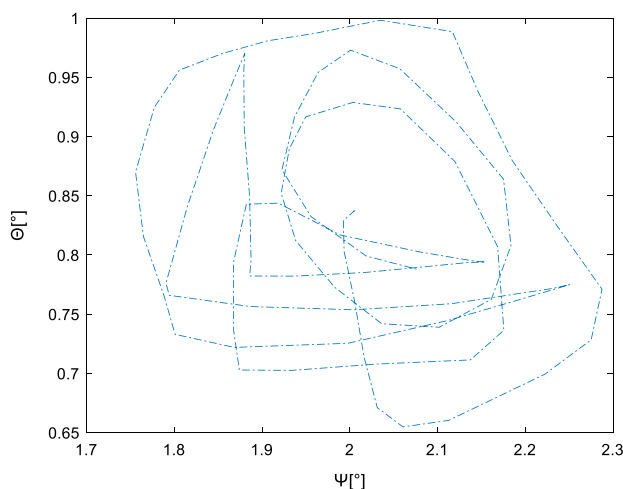
**Figure 19.** Trajectory obtained from a recorded surgeon gesture by motion capture.

Fig. 18 $N(N_x, N_y)$. Both the analytic and the simulation forces were calculated using the serial chain and the parallel chain of the nHH device.

As follows from the table shown above, we manage to prove that the proposed HH device has a good force feedback and capable to regenerate the force applied by the surgeon in order to stimulate the real and the virtual environment. Despite the fact that the chosen points where we calculate the force feedback are at the edges of the workspace (with an altered dexterity index), we still manage to have suitable feedback where the error does not exceed 2% for a force applied along the X axis as presented in Fig. 18.

The next a comparison between the nHH and the SPM [12, 38] devices is performed. The SPM, as the nHH device, is meant to be used as a haptic device in robotic system for minimally invasive surgery application. In order to prove the efficiency of the proposed architecture of nHH device, a comparison study is proposed [39].

The comparison of the two manipulators is based on the capability of each device to perform motions around a specific point in its workspace. Dexterity, which represent the amplification of errors as a result of kinematic and static transformation between cartesian and joints spaces, is chosen to evaluate the kinematic for each manipulator. For the SPM, the dexterity has been calculated and determined by Saafi [13, 23].

Based on results in [23], the maximum value of the dexterity that can be reached is about 0.4 at the center of the workspace with a self-rotation $\varphi = 0^\circ$.

The comparison is based on choosing a recorded trajectory in the workspace of both manipulators, then calculate the dexterity along this path. The trajectory has been obtained during a recorded surgeon motion in a real mini-invasive surgery task using a motion capture system [24]. Figure 19 gives a graphical representation of the trajectory in the plane (ψ, θ) .

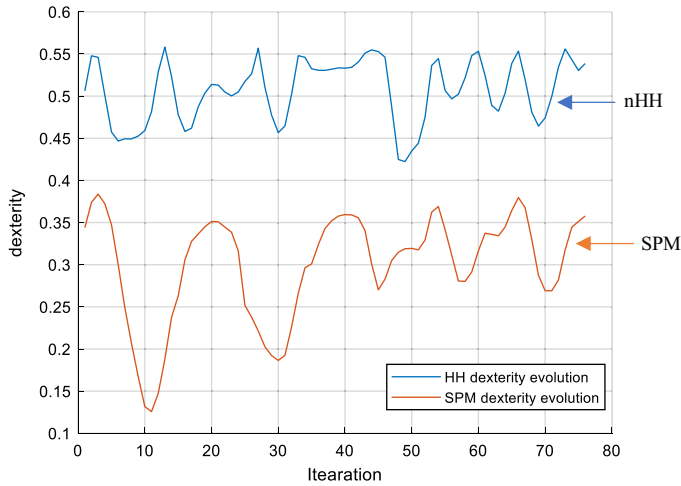


Figure 20. Dexterity evolution for nHH and SPM for $\phi = 0^\circ$.

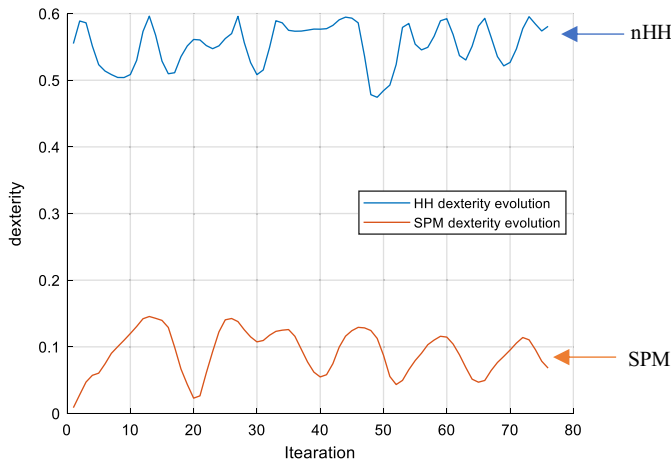


Figure 21. Dexterity evolution for nHH and SPM for $\phi = 50^\circ$.

The same trajectory was implemented on the nHH device. The obtained results for different values of self-rotation, $\varphi = 0^\circ$, $\varphi = 50^\circ$, and $\varphi = -10^\circ$, are shown in Figs. 20, 21 and 22, respectively.

Table III resumes the maximum, minimum and mean dexterity along the chosen trajectory for both manipulators with a self-rotation $\phi = 0^\circ$.

Table IV resume dexterity values along the chosen trajectory for both manipulators with a self-rotation $\phi = 50^\circ$.

Table V resume dexterity values along the chosen trajectory for both manipulators with a self-rotation $\phi = -10^\circ$.

For a self-rotation $\phi = 0^\circ$ and along the chosen trajectory, the SPM’s dexterity goes from 0.38 to 0.12. This is explained by the presence of singularities inside the workspace that alters the kinematic performance and amplifies the errors. Moreover, near singular configurations, the self-rotation is no more controllable. However, the nHH device represents a good dexterity along the same trajectory which can reach 0.55 at it is maximum.

Consider Fig. 21, which plots the SPM’s dexterity against the nHH’s dexterity for a self-rotation $\phi = 50^\circ$. From the resulting plot, we can confirm that the SPM have a bad kinematic performance. The

Table III. *Dexterity values for SPM and nHH device for $\phi = 0^\circ$.*

	Max	Min	Mean
SPM	0.3838	0.1258	0.3001
nHH	0.5581	0.4223	0.5071

Table IV. *Dexterity values for SPM and nHH device for $\phi = 50^\circ$.*

	Max	Min	Mean
SPM	0.1455	0.0087	0.0924
HH	0.5962	0.4744	0.5536

Table V. *Dexterity values for SPM and HH device for $\phi = -10^\circ$.*

	Max	Min	Mean
SPM	0.3920	0.1255	0.3016
HH	0.4495	0.3412	0.4066

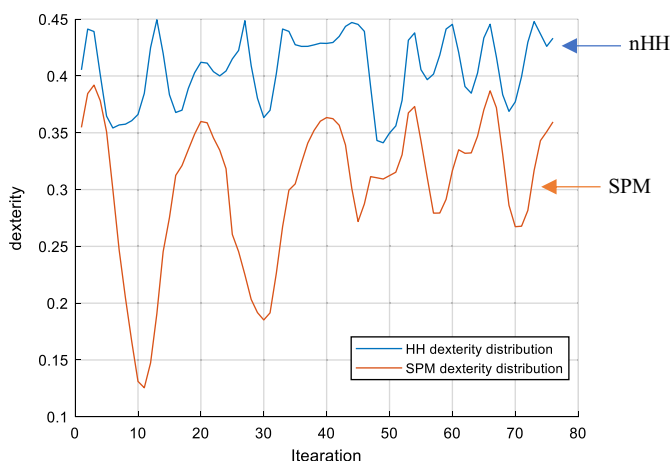


Figure 22. *Dexterity evolution for HH and SPM for $\phi = -10^\circ$.*

new haptic device presents a maximum dexterity of 0.59. This value is greater than the SPM's which is limited to 0.3.

According to the results presented above by the three figures and the three tables, the suitability and potential of the novel architecture as a haptic interface for surgical tasks. Since the dexterity of the nHH device is above 0.3412 for the different orientations and along the chosen trajectory, the new hybrid manipulator is adequate for many tasks, especially for minimally invasive surgical ones.

6. Conclusion

In this paper, we proposed a new hybrid haptic (nHH) device with a fixed center of rotation and 4-doF. The nHH is designed to be used as a master device in robotic platform dedicated to laparoscopic surgery. The proposed device is an association of two chains, a serial and a parallel chain. The serial

chain (SC) allows to handle the translational motion (1-dof) and the parallel chain (PC) allows to handle the rotational motion (3-dofs), mainly the two tilt motions and the self-rotation.

The geometric parameters of the nHH device were optimized in order to fit the task workspace as well as a best kinematic performance distribution over its workspace. Global dexterity has been chosen as a criterion to characterize this kinematic performance. A safety margin distance is included in the optimization to eliminate singular region from the workspace. A kinematic model of the nHH device has been developed and validated using a SimMechanics model.

A comparison study has been performed between the proposed device and a SPM dedicated to a similar application. A real surgeon gesture is considered for the orientation of the master device. The results obtained prove that the nHH device presents a more interesting behavior than the SPM and still far from singularity. The global dexterity index is over 0.5 and its value is not altered by the self-rotation, which is one of the major limitations of the SPM.

The CAD model and first prototype of the nHH device are presented and will be used in future work which will be focused on the master-slave scheme and haptic control implementation.

Authors' contributions. M.M., H.S., A.M., M.A., and M.A.L. conceived and designed the study. M.M., M.A., and M.A.L. conducted and analyzed the numerical experiments. M.M., H.S., A.M., M.A., S.Z., and M.A.L. wrote the article.

Financial support. This work was financially supported by the "IRP-RACeS" program IRP: Robotic Assisted System for Safe Cervical Surgery supported by the CNRS in France and European program of international students' mobility.

Ethical considerations. None.

Competing interests. The authors declare no competing interests.

References

- [1] S. Kansal, M. Zubair, B. Suthar and S. Mukherjee, "Tele-operation of an industrial robot by an arm exoskeleton for peg-in-hole operation using immersive environments," *Robotica* **40**(2), 234–249 (2022).
- [2] R. E. Ellis, O. M. Ismaeil and M. G. Lipssett, "Design and Evaluation of a High-Performance Prototype Planar Haptic Interface," *In: American Society of Mechanical Engineers, Dynamic Systems and Control Division (Publication) DSC*, vol. 49 (1993) pp. 55–64.
- [3] W. Park, L. Kim, H. Cho and S. Park, "Design of Haptic Interface for Brickout Game," *In: 2009 IEEE International Workshop on Haptic Audio Visual Environments and Games, HAVE 2009 - Proceedings* (2009) pp. 64–68.
- [4] H. Kandemir and H. Kose, "Development of adaptive human-computer interaction games to evaluate attention," *Robotica* **40**(1), 56–76 (2022).
- [5] J. Broeren, M. Rydmark and K. S. Sunnerhagen, "Virtual reality and haptics as a training device for movement rehabilitation after stroke: A single-case study," *Arch. Phys. Med. Rehabil.* **85**(8), 1247–1250 (2004).
- [6] G. S. Giri, Y. Maddahi and K. Zareinia, "An application-based review of haptics technology," *Robotics* **10**(1), 1–18 (2021).
- [7] M. Karkoub, M. G. Her and J. M. Chen, "Design and control of a haptic interactive motion simulator for virtual entertainment systems," *Robotica* **28**(1), 47–56 (2010).
- [8] F. Gosselin, T. Jouan, J. Brisset and C. Andriot, "Design of a Wearable Haptic Interface for Precise Finger Interactions in Large Virtual Environments," *In: Proceedings - First Joint Eurohaptics Conference and Symposium on Haptic Interfaces for Virtual Environments and Teleoperator Systems. World Haptics Conference, WHC 2005* (2005) pp. 202–207.
- [9] I. F. Zidane, Y. Khattab, S. Rezeka and M. El-Habrouk, "Robotics in laparoscopic surgery - A review," *Robotica* **41**(1), 126–173 (2023).
- [10] H. Feedback, L. Van Den Bedem, R. Hendrix, N. Rosielle, M. Steinbuch and H. Nijmeijer, "Design of a Minimally Invasive Surgical Teleoperated Master-Slave System with Design of a Minimally Invasive Surgical Teleoperated Master-Slave System with Haptic Feedback," *In: 2009 International Conference on Mechatronics and Automation* (2009).
- [11] A. Chaker, A. Mlika, M. A. Laribi, L. Romdhane and S. Zeghloul, "Synthesis of spherical parallel manipulator for dexterous medical task," *Front. Mech. Eng.* **7**(2), 150–162 (2012).
- [12] H. Saafi, M. A. Laribi and S. Zeghloul, "Optimal Haptic Control of a Redundant 3-RRR Spherical Parallel Manipulator," *In: IEEE International Conference on Intelligent Robots and Systems* (2015) pp. 2591–2596.
- [13] H. Saafi, M. A. Laribi and S. Zeghloul, "Redundantly actuated 3-RRR spherical parallel manipulator used as a haptic device: Improving dexterity and eliminating singularity," *Robotica* **33**(5), 1113–1130 (2015).
- [14] H. Saafi, M. A. Laribi and S. Zeghloul, "Improvement of the Direct Kinematic Model of a Haptic Device for Medical Application in Real Time Using an Extra Sensor," *In: International Conference on Intelligent Robots and Systems* (2014) pp. 1697–1702.

- [15] H. Saafi, M. Vulliez, S. Zeghloul and M. A. Laribi, "A new serial approach of the forward kinematic model of spherical parallel manipulators for real-time applications," *Proc. Inst. Mech. Eng. C J. Mech. Eng. Sci.* **232**(4), 677–684 (2018).
- [16] M. Meskini, H. Saafi, M. A. Laribi, A. Mlika, M. Arsicault and S. Zeghloul, "Serial approach for solving the forward kinematic model of the DELTA robot," *Mech. Mach. Sci.* **103**, 305–312 (2021).
- [17] C. Preaúlt, H. Saafi, M. A. Laribi and S. Zeghloul, "Optimal design and evaluation of a dexterous 4 DoFs haptic device based on delta architecture," *Robotica* **37**(7), 1267–1288 (2019).
- [18] T. K. Tanev, "Kinematics of a hybrid (parallel-serial) robot manipulator," *Mech. Mach. Theory* **35**(9), 1183–1196 (2000).
- [19] P. Xu, C. F. Cheung, C. Wang and C. Zhao, "Novel hybrid robot and its processes for precision polishing of freeform surfaces," *Precis. Eng.* **64**, 53–62 (2020).
- [20] F. Ennaïem, Chaker A., Sandoval J., Mlika A., Romdhane L., Bennour S., Zeghloul S. and Laribi M. A., "A hybrid cable-driven parallel robot as a solution to the limited rotational workspace issue," *Robotica* **41**(3), 1–19 (2022).
- [21] G. Carbone and M. Ceccarelli, "A stiffness analysis for a hybrid parallel-serial manipulator," *Robotica* **22**(5), 567–576 (2004).
- [22] H. Saafi, M. A. Laribi and S. Zeghloul, "Design of a 4-DoF (degree of freedom) hybrid-haptic device for laparoscopic surgery," *Mech. Sci.* **12**(1), 155–164 (2021).
- [23] H. Saafi, M. A. Laribi and S. Zeghloul, "Forward kinematic model improvement of a spherical parallel manipulator using an extra sensor," *Mech. Mach. Theory* **91**, 102–119 (2015).
- [24] M. A. Laribi, T. Riviere, M. Arsicault and S. Zeghloul, "A New Teleoperated Robotic System for Minimally Invasive Surgery: Modeling and Identification," **In: 2013 International Conference on Control, Decision and Information Technologies, CoDIT 2013** (2013) pp. 659–664.
- [25] M. A. Laribi, M. Arsicault, T. Riviere and S. Zeghloul, "Toward New Minimally Invasive Surgical Robotic System," **In: 2012 IEEE International Conference on Industrial Technology, ICIT 2012, Proceedings** (2012) pp. 504–509.
- [26] M. A. Laribi, T. Riviere, M. Arsicault and S. Zeghloul, "A Design of Slave Surgical Robot Based on Motion Capture," **In: 2012 IEEE International Conference on Robotics and Biomimetics, ROBIO 2012 - Conference Digest** (2012) pp. 600–605.
- [27] S. Nisar, T. Endo and F. Matsuno, "Design and kinematic optimization of a two degrees-of-freedom planar remote center of motion mechanism for minimally invasive surgery manipulators," *J. Mech. Robot.* **9**(3), 1–9 (2017).
- [28] J. Kucuk, "Energy minimization for 3-RRR fully planar parallel manipulator using particle swarm optimization," *Mech. Mach. Theory* **62**, 129–149 (2013).
- [29] J. Angeles, "A global performance index for the kinematic optimization of robotic manipulators," *J. Mech. Des. Trans. ASME* **113**(3), 220–226 (1991).
- [30] T. Essomba and L. N. Vu, "Kinematic analysis of a new five-bar spherical decoupled mechanism with two-degrees of freedom remote center of motion," *Mech. Mach. Theory* **119**, 184–197 (2018).
- [31] T. Yoshikawa, "Manipulability of robotic mechanisms," *Int. J. Robot. Res.* **4**(2), 3–9 (1985).
- [32] J. Angeles, F. Ranjbaran and R. V. Patel, "On the Design of the Kinematic Structure of Seven-Axes Redundant Manipulators for Maximum conditioning," **In: Proceedings - IEEE International Conference on Robotics and Automation**, vol. 1 (1992) pp. 494–499.
- [33] S. M. Shorman and S. A. Pitchay, "Significance of parameters in genetic algorithm, the strengths, its limitations and challenges in image recovery," *ARNP J. Eng. Appl. Sci.* **10**(2), 585–593 (2015).
- [34] R. Kelaiaia, O. Company and A. Zaatri, "Multiobjective optimization of parallel kinematic mechanisms by the genetic algorithms," *Robotica* **30**(5), 783–797 (2012).
- [35] S. Zeghloul and P. Rambeaud, "A fast algorithm for distance calculation between convex objects using the optimization approach," *Robotica* **14**(4), 355–363 (1996).
- [36] J. H. Holland, "Genetic Algorithms and Adaptation," **In: Adaptive Control of Ill-Defined Systems, Nato Conference Series** (O. G. Selfridge, E. L. Rissland and M. A. Arbib, eds.), vol. 16 (Springer, Boston, MA, 1984) pp. 317–333.
- [37] D. E. Goldberg, "Genetic Algorithms in Search, Optimization, and Machine Learning," **In: American Society of Mechanical Engineers, Dynamic Systems and Control Division (Publication) DSC**, vol. 22 (1990) pp. 39–45.
- [38] D. Zhang, Z. Xu, C. M. Mechefske and F. Xi, "Optimum design of parallel kinematic toolheads with genetic algorithms," *Robotica* **22**(1), 77–84 (2004).
- [39] H. Saafi and H. Lamine, "Comparative kinematic analysis and design optimization of redundant and nonredundant planar parallel manipulators intended for haptic use," *Robotica* **38**(8), 1463–1477 (2020).